Electronic Supplementary Material (ESI) for ChemComm.
This journal is © The Royal Society of Chemistry 2014

ELECTRONIC SUPPORTING INFORMATION FOR:

Self-organization of star-shaped columnar liquid crystals with a coaxial nanophase segregation revealed by a combined experimental and simulation approach

Eduardo Beltrán,[a] Matteo Garzoni,[b] Beatriz Feringán,[a] Alberto Vancheri,[b] Joaquín Barberá,[a] José Luis Serrano,[a] Giovanni M. Pavan,*[b] Raquel Giménez*[a] and Teresa Sierra*[a]

[a] *Departamento de Química Orgánica, Instituto de Ciencia de Materiales de Aragón (ICMA) - Facultad de Ciencias, CSIC - Universidad de Zaragoza, 50009 Zaragoza, Spain.*

[b] *Department of Innovative Technologies, University of Applied Sciences and Arts of Southern Switzerland, Galleria 2, Manno 6928, Switzerland.*

Contents

1. Scheme S1. Synthetic procedures for the preparation of T-TPC$_6$ and T-TPC$_{10}$.

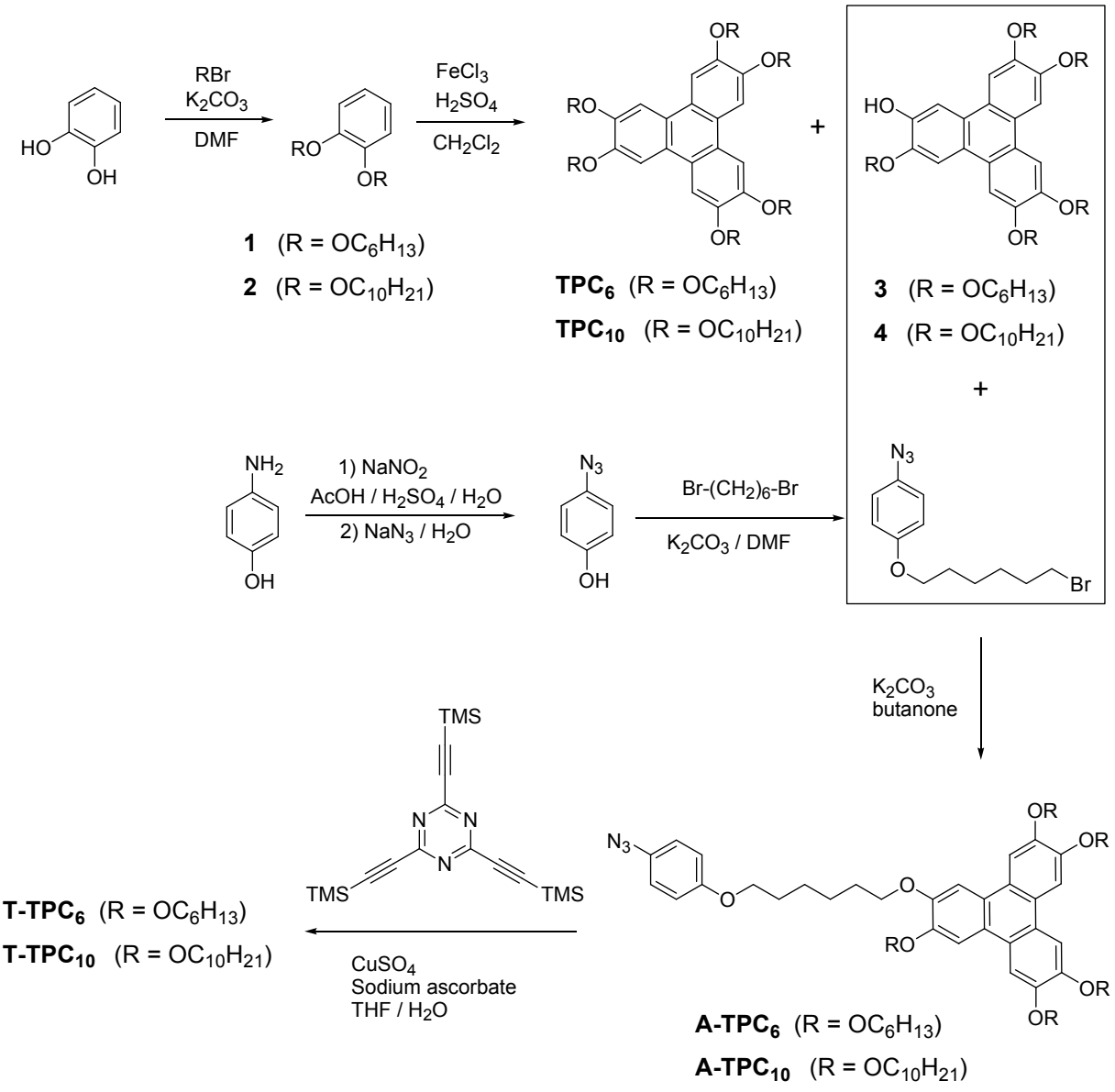

2. Synthesis and characterization data.

General procedure for the synthesis of monohydroxylated compounds 3 and 4.

The synthesis of the monohydroxypentaalkoxytriphenylenes (**3**, **4**) was approached in one step from dialkoxylated benzenes (**1**, **2**). In this way mixtures of hexaalkoxytriphenylenes (**TPC_6** or **TPC_{10}**) and monohydroxypentaalkoxytriphenylenes (**3** or **4**) were obtained, which were easily separated by column chromatography with yields of 54 % and 21 % respectively.

4.3 mmol of (**1)** or **(2)**[1] and catalytic sulphuric acid (2 drops) were added to anhydrous dichloromethane (75 mL). Then, 12.9 mmol $FeCl_3$ was added slowly to the reaction mixture and the reaction was stirred for 24 hours. The mixture was poured carefully into stirred MeOH (60 mL), the mixture left for 1 h and then allowed to cool overnight in a refrigerator. The solid was filtered off, washed with cold MeOH and purified by column chromatography.

2,3,6,7,10-Penta(hexyloxy)-11-hydroxytriphenylene (3) was purified by column chromatography with hexane / ethyl acetate 9 / 1 as eluent as a off-white solid. Yield: 21 %. ^{1}H NMR (400 MHz, $CDCl_3$) δ, ppm 0.89 (m, 15H), 1.36–1.42 (m, 20H), 1.53-1.61 (m, 20H), 1.90-1.99 (m, 10H), 4.23 (t, *J* = 6.6 Hz, 8H), 4.29 (t, *J* = 6.5 Hz, 2H), 5.91 (s, 1H), 7.77 (s, 4H), 7.82-7.83 (m, 4H), 7.96 (s, 1H); R_f = 0.47 (hexane / ethyl acetate 9 / 1).

2,3,6,7,10-Penta(decyloxy)-11-hydroxytriphenylene (4) was purified by column chromatography with hexane/ethyl acetate 9.5/0.3 as eluent to give a off-white solid. Yield: 23 %. ^{1}H NMR (400 MHz, $CDCl_3$) δ, ppm 0.89 (t, *J* = 6.5 Hz, 15H), 1.29–1.42 (m, 60H), 1.52-1.61 (m, 10H), 1.90-1.97 (m, 10H), 4.23 (t, *J* = 6.8 Hz, 8H), 4.28 (t, *J* = 6.5 Hz, 2H), 5.91 (s, 1H), 7.77 (s, 4H), 7.81-7.84 (m, 4H), 7.96 (s, 1H); R_f = 0.11 (hexane / ethyl acetate 9.5 / 0.3).

2,3,6,7,10,11-Hexa(hexyloxy)triphenylene (TPC_6) was purified by column chromatography with hexane / ethyl acetate 9 / 1 as eluent to give **5** as a off-white solid. Yield: 53 %. ^{1}H NMR (400 MHz, $CDCl_3$) δ, ppm 0.89 (t, *J* = 6.9 Hz, 18H), 1.36–1.47 (m, 12H), 1.52-1.62 (m, 12H), 1.90-1.97 (m, 12H), 4.23 (t, *J* = 6.8 Hz, 12H), 7.84 (s, 6H); R_f = 0.70 (hexane / ethyl acetate 9 / 1)

2,3,6,7,10,11-Hexa(decyloxy)triphenylene (TPC_{10}) was purified by column chromatography with hexane / ethyl acetate 9.5 / 0.3 as eluent to give **6** as a off-white solid. Yield: 55 %. ^{1}H NMR (300 MHz, $CDCl_3$) δ, ppm 0.80-0.93 (m, 18H), 1.20-1.41 (m, 72H), 1.49-1.65 (m, 12H), 1.85-1.99 (m, 12H), 4.15-4.30 (m, 12H), 7.83 (s, 6H); R_f = 0.22 (hexane / ethyl acetate 9.5 / 0.3)

Synthesis of 1-Azido-4-((6-bromohexyl)oxy)benzene) 0.6 mmol of 4-azidophenol[2] and 3.5 mmol of dry potassium carbonate were dissolved in 15 mL of dry butanone. Under reflux conditions 0.6 mmol of 1,6-dibromohexane were added and the reaction mixture was stirred for 24 hours. The crude was purified by column chromatography with hexane as eluent. Yield: 66 %. ^{1}H NMR (400 MHz, $CDCl_3$) δ, ppm 1.23-1.31 (m, 2H), 1.46-1.56 (m, 2H), 1.75-1.94 (m, 4H), 3.42 (t, *J* = 6.8 Hz, 2H), 3.93 (t, *J* = 6.4 Hz, 2H), 6.86-6.89 (m, 2H), 6.93-6.96 (m, 2H);^{13}C NMR (100 MHz, $CDCl_3$) δ, ppm 22.6, 25.2, 27.9, 29.0, 32.6, 33.6, 68.0, 115.6, 119.9, 132.2, 156.4; R_f = 0.54 (hexane).

General procedure for the synthesis of azide precursors A-TPC$_6$ and A-TPC$_{10}$

0.17 mmol of 2,3,6,7,10-Penta(hexyloxy)-11-hydroxytriphenylene (**3**) or 2,3,6,7,10-penta(decyloxy)-11-hydroxytriphenylene (**4**), 1.0 mmol of dry potassium carbonate and 0.17 mmol of 1-azido-4-((6-bromohexyl)oxy)benzene) were added to dry butanone (30 mL). The mixture was heated under reflux for 24 h, after which it was hot-filtered and the acetone removed under reduced pressure to leave an off-white solid. The product was purified by column chromatography with silica gel as stationary phase and the suitable eluent. Compounds are quickly used in the next step.

2-((5-(4-azidophenyl)hexyl)oxy)-3,6,7,10,11-pentakis(hexyloxy)triphenylene (A-TPC$_6$) was purified by column chromatography with hexane / ethyl acetate 9 / 1 as eluent. Yield: 48 %. ^{1}H NMR (400 MHz, $CDCl_3$) δ, ppm 0.92-0.95 (m, 15H), 1.35-1.45 (m, 20H), 1.52-1.62 (m, 14H), 1.88-1.99 (m, 14H), 3.96 (t, *J* = 6.4 Hz, 2H), 4.21-4.26 (m,12H), 6.85-6.88 (m, 2H), 6.92-6.94 (m, 2H), 7.84 (s, 6H); ^{13}C NMR (100 MHz, $CDCl_3$) δ, ppm 14.0, 22.6, 25.8, 29.4, 31.7, 68.2, 69.5, 69.6, 69.7, 69.8, 107.2, 107.3, 107.4, 115.7, 119.9, 123.6, 123.7, 148.8, 148.9, 149.0, 156.5; IR (NaCl) υ (cm^{-1}) 2918, 2850 (C-C), 2112 (N_3), 1610, 1523, 1504 (arC-C), 1256 (C-O); MS (MALDI+, dithranol): 935.9 $[M\text{-}N_2\text{+}2H]^+$, 920.9 $[M\text{-}N_3\text{+}H]^{+\cdot}$, 844.8 $[M\text{-}N_3Ph\text{+}H]^{+\cdot}$, 744.8 $[M\text{-}N_3PhOC_6H_{12}\text{+}H]^{+\cdot}$(Calcd for $C_{60}H_{87}N_3O_7$: 961.6); Rf = 0.48 (hexane / ethyl acetate 9 / 1)

2-((5-(4-azidophenyl)hexyl)oxy)-3,6,7,10,11-pentakis(decyloxy)triphenylene (A-TPC$_{10}$) was purified by column chromatography with hexane / ethyl acetate 10 / 0.5 as eluent. Yield: 95 %. ^{1}H NMR (400 MHz, $CDCl_3$) δ, ppm 0.88-0.92 (m, 15H), 1.24-1.38 (m, 60H), 1.52-1.65 (m, 14H), 1.71-2.00 (m, 14H), 3.89-3.97 (m, 2H), 4.21-4.29 (m,12H), 6.86-6.88 (m, 2H), 6.92-6.94 (m, 2H), 7.86 (s, 6H); ^{13}C NMR (100 MHz, $CDCl_3$) δ, ppm 14.1, 22.7, 26.2, 29.4, 29.5, 29.6, 29.7, 31.9, 68.2, 69.5, 69.6, 69.7, 69.8, 69.9, 104.3, 106.4, 107.2, 107.3, 107.4, 107.6, 115.6, 119.9, 122.9, 123.2, 123.6, 123.9, 132.1, 145.2, 145.8, 148.8, 149.0, 156.4; IR (NaCl) υ (cm^{-1}) 2917, 2849 (C-C), 2112 (N_3), 1611, 1520, 1506 (arC-C), 1257 (C-O); MS (MALDI+, dithranol): 1239.2 [M-

N_2+2H+Na]$^+$, 1216.3 [M-N_2+2H]$^{+\cdot}$, 1025.1 [M-$N_3PhOC_6H_{12}O$]$^{+\cdot}$(Calcd for $C_{80}H_{127}N_3O_7$: 1242.0). Rf = 0.34 (hexane / ethyl acetate 9 / 0.5).

General procedure for the synthesis of compounds T-TPC$_6$ and T-TPC$_{10}$

0.06 mmol of 2,4,6-tris[(trimethylsilyl)ethynyl]-1,3,5-triazine[3] and 0.18 mmol of azide **A-TPC$_6$** or **A-TPC$_{10}$** were dissolved in a mixture THF / H_2O (2 mL / 2 mL). The solution was stirred for 3 minutes. Then, 0.02 mmol of sodium ascorbate, $9\cdot10^{-3}$ mmol of copper(II) sulphate and 0.18 mmol of TBAF 1 M in THF were added. The flask was kept in dark for 12 hours. The reaction mixture was extracted with dichloromethane / water 2 / 1 (3x10 mL) and the combined organic layers were dried over $MgSO_4$. The solvent was evaporated, and the residue was purified by column chromatography with silica gel as the stationary phase and the suitable eluent.

2,4,6-tris(1-(4-((6-((3,6,7,10,11-pentakis(hexyloxy)triphenylen-2-yl)oxy)hexyl)oxy)phenyl)-1*H*-1,2,3-triazol-4-yl)-1,3,5-triazine (T-TPC$_6$) was purified by column chromatography with dichloromethane / ethyl acetate as eluent (10 / 0.5). Yield: 30 %. ^{1}H NMR (400 MHz, $CDCl_3$) δ, ppm 0.82-0.95 (m, 45H), 1.29-1.44 (m, 60H), 1.48-1.59 (m, 42H), 1.84-1.99 (m, 42H), 4.0-4.1 (m, 6H), 4.14-4.28 (m, 36H), 7.03-7.09 (m, 6H), 7.71-7.87 (m, 24H), 9.10 (s, 3H, triazole); ^{13}C NMR (100 MHz, $CDCl_3$) δ, ppm 14.0, 22.6, 25.8, 25.9, 29.2, 29.4, 29.6, 31.6, 60.3, 68.3, 69.4, 69.5, 69.6, 69.7, 107.1, 107.2, 107.3, 115.3, 122.3, 123.5, 123.6, 125.0, 128.8, 129.8, 130.9, 135.1, 145.7, 148.8, 148.9, 149.0, 159.8, 166.8, 166.5, 171.1, 183.6; Anal. Calcd for $C_{189}H_{264}N_{12}O_{21}$: C, 74.67; H, 8.75; N, 5.53 Found: C, 74.58; H, 8.85; N, 5.26; MS (MALDI+, dithranol): 3039.9 [M]$^{+\cdot}$ (Calcd for $C_{189}H_{264}N_{12}O_{21}$: 3040.0), Rf = 0.35 (dichloromethane / ethyl acetate 10 / 0.5).

2,4,6-tris(1-(4-((6-((3,6,7,10,11-pentakis(decyloxy)triphenylen-2-yl)oxy)hexyl)oxy)phenyl)-1*H*-1,2,3-triazol-4-yl)-1,3,5-triazine (T-TPC$_{10}$) was purified by column chromatography with dichloromethane / ethyl acetate as eluent (10 / 0.5). Yield: 35 %. ^{1}H NMR (400 MHz, $CDCl_3$) δ, ppm 0.80-0.92 (m, 45H), 1.19-1.38 (m, 180H), 1.50-1.63 (m, 42H), 1.85-2.00 (m, 42H), 4.0-4.1 (m, 6H), 4.14-4.28 (m,36H), 7.05-7.08 (m, 6H), 7.74-7.74 (m, 6H), 7.84 (s, 18H), 9.09 (s, 3H, triazole); ^{13}C NMR (100 MHz, $CDCl_3$) δ, ppm 14.1, 22.7, 23.4, 25.9, 26.0, 26.2, 26.4, 29.4, 29.5, 29.6, 29.7, 31.9, 68.4, 69.5, 69.6, 69.7, 69.8, 107.2, 107.3, 107.4, 107.5, 115.4, 122.2, 123.5, 123.6, 123.7, 125.0, 129.4, 129.8, 135.2, 145.7, 148.8, 148.9, 149.0, 159.8, 166.7; Anal. Calcd for $C_{189}H_{264}N_{12}O_{21}$: C, 77.04; H, 9.97; N, 4.33 Found: C, 77.02; H, 9.92; N, 4.20; MS (MALDI+, dithranol): 3880.5 [M]$^{+\cdot}$(Calcd for $C_{249}H_{384}N_{12}O_{21}$: 3880.9), Rf = 0.30 (dichloromethane / ethyl acetate 9 / 0.5).

3. General Experimental Methods

^{1}H-NMR and ^{13}C-NMR experiments were performed on a Bruker ARX 300 or a Bruker AVANCE 400 spectrometer. Chemical shifts are given in ppm relative to TMS, and the solvent residual peak was used as internal standard ($CDCl_3$ δ_H = 7.26 ppm, δ_C = 77.0 ppm). MS analyses were performed using a Bruker Microflex spectrometer. Elemental analyses were performed using a Perkin-Elmer 2400 microanalyzer. IR spectra on NaCl pellets were recorded using a Thermo Nicolet Avatar 380 spectrophotometer. Liquid crystal behavior were studied using an Olympus BH-2 polarizing microscope equipped with a Linkam TMS91 hot-stage and a CS196 hot-stage central processor. DSC TA Instruments Q-20 and Q-2000 systems were used to carry out differential scanning calorimetry experiments. Samples were sealed in aluminum pans, and measured at a scanning rate of 10 ºC min^{-1} under a nitrogen flow. Temperatures were taken from the onset of the transition unless otherwise noted. X-ray diffraction experiments of the mesophases were performed in a pinhole camera (Anton-Paar) operating with a point focused Ni filtered Cu-Kα beam. Lindemann glass capillaries with 0.9 mm inner diameter were used to contain the sample and heated, when necessary, with a high-temperature attachment. The capillary axis was held perpendicular to the X-ray beam and the pattern collected on flat photographic film. Bragg´s law was used to calculate the *d* spacings.

4. Liquid crystal properties

DSC thermograms run at 10 ºC min^{-1} do not show clear transitions on cooling as the mesophases develop very slowly and need an annealing process, as observed by POM. Therefore, in Table S1 only POM temperatures of the isotropic liquid-to-mesophase transition in the cooling process are shown.

Compound T-TPC_6 was obtained as a crystalline solid that melts at 56 ºC to the liquid crystal phase in the first heating and does not crystallize in subsequent cycles (Figure S2, a). The compound remained without crystallizing for long periods of time.

Compound T-TPC_{10} was obtained as a waxy material that is mesomorphic and for which a clear melting or crystallization has not been observed in DSC cycles. Only a broad clearing transition is observed in the heating cycle (Figure S2, b).

The X-ray measurements on the mesophases were carried out at room temperature after the thermal treatment of the samples. This is consistent with the fact that no crystallization was observed in the cooling process by DSC or by optical microscopy, and suggests that the mesophase is preserved in a glassy state.

Table S1. Phase transitions and XRD parameters

Compound	Phase transition[a] T (ºC)	d_{meas} (Å) [b]	hkl	d_{calc} (Å)	Parameters (Å)
T-TPC_6	I 90 Col_h	45.4	100	45.4	a = 52.6
		17.3	210	17.2	c = 4.1
		4.7	(broad halo)		
		4.1	001		
T-TPC_{10}	I 118 Col_r	47.0	110	47.0	a = 80.2
		29.0	020	29.0	b = 58.0
		23.7	220	23.5	c = 3.5
		19.6	400	20.0	
		15.8	330	15.7	
		4.4	(broad halo)		
		3.5	001		

[a] POM data for the first cooling cycle. Cr = crystal, Col_h = hexagonal columnar mesophase, Col_r = rectangular columnar mesophase, I = isotropic liquid. [b] Data obtained from slow cooled samples from the isotropic liquid up to 80 ºC and then fast cooled to room temperature.

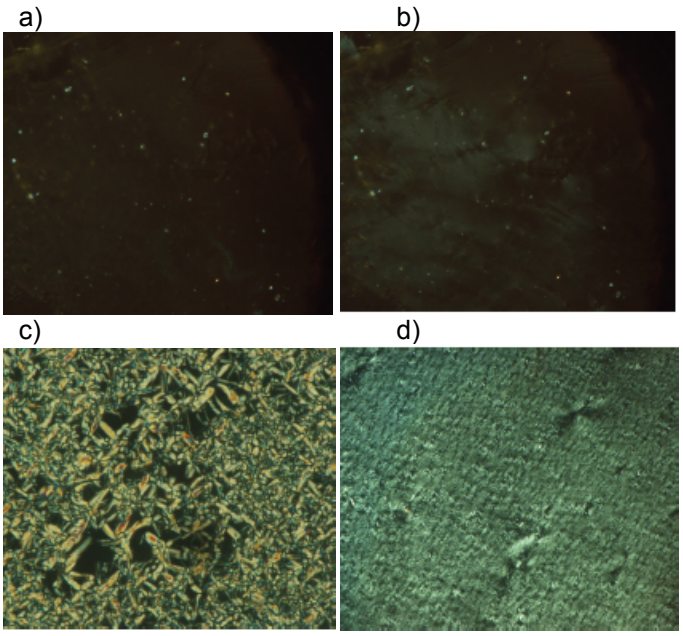

Figure S1. Microphotographs of the textures observed at the optical microscope under crossed polarizers, a) **T-TPC$_6$** at 20 ºC, b) T-TPC$_6$ at 20 ºC after shearing, c) **T-TPC$_{10}$** at 90 ºC, d) **T-TPC$_{10}$** at 20 ºC after shearing.

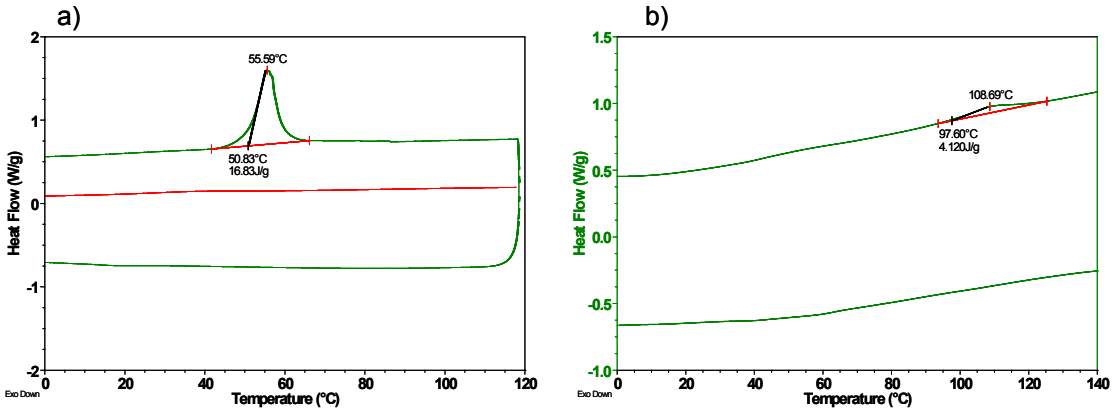

Figure S2. DSC trace (green: first heating-cooling cycle, red: second heating cycle) for a) **T-TPC$_6$**, b) **T-TPC$_{10}$**

5. Self-assembly models from XRD

The rectangular symmetry of the mesophase of **T-TCP$_{10}$** corresponds to a distorted hexagonal lattice. Let us recall that a hexagonal network is a particular case of rectangular network with a/b = √3. For **T-TCP$_{10}$** a/b < √3 and therefore the symmetry is not hexagonal any longer. The distorsion could be associated to a tilting of the discotic units; however no information about the existence of tilting can be drawn from the X-ray measurements. In this case the disks are represented by circles as denote the centers of mass of the columns.

Figure S3. Enlarged view of the self-assembly models. a) **T-TPC$_6$**, b) **T-TPC$_{10}$**. Blue and red dots represent the centers of mass of the columns.

6. Computational procedure

The computational strategy used in this work is consistent with the approach adopted in previous reports for the study of liquid crystals[4] and of other ordered soft nanostructures in solution.[5]

The molecular models for the **T-TPC$_6$** and **T-TPC$_{10}$** simulated systems were obtained starting from initially extended and planar **T-TPC$_6$** and **T-TPC$_{10}$** supermolecules replicated in space according to the assembling schemes proposed by the XRD experiments (Fig. 2 in the main paper and Figure S3). In the case of **T-TPC$_6$**, two

molecules were initially arranged in each blue node according to the scheme reported above. In the case of **T-TPC$_{10}$**, the three empty positions in a stratum of the column are occupied by red groups (triphenylene) from the neighbor columns in the rectangular lattice. The simulated molecular systems are composed of four columns containing 36 **T-TPC$_{10}$** molecules, or 72 **T-TPC$_6$** (two molecules for each node), arranged in space consistent with the lattice parameters (*a*, *b* and *c*) obtained from XRD experiments (see Table S2 for details). The initial distances between the columns, and between the molecules in the each column, were slightly increased (in percentage) to avoid initial local superpositions (Table S2).[4] For what pertains to the initial configurations of the **T-TPC$_{10}$–0°** and **T-TPC$_6$–0°** superimposed systems, the supermolecules in the same column are simply translated along the *z* axis (Fig. 3a and Fig. 4a in the main paper). On the other hand, in the symmetric rotated systems, **T-TPC$_{10}$–180°** and **T-TPC$_6$–60°**, the supermolecules in each layer are rotated respect to the neighbors along the *z* axis by 180° or 60° respectively. In this way, the rectangular and hexagonal symmetries of the lattices are fully respected, but the extended supermolecules are initially staggered along the *z* axis (Fig. 3b and Fig. 4b in the main paper). The molecular dynamics (MD) simulations of the four systems were conducted in periodic boundary conditions, so that the created molecular systems replicated in space are effectively infinite in the *x*, *y* and *z* directions, and are representative of the bulk ordered phase of the liquid crystals (Fig. 3a,b and Fig 4a,b in the main paper). Table S2 reports the main features of the molecular systems simulated in this work.

Table S2. Main features of the molecular systems simulated in this study.

Molecular system	Number of columns in the system[a]	Number of molecules in each column [b]	Total number of molecules in the system	Rotation angle between neighbor molecules along the *z* axis [c]	Initial box size [d] (Å x Å x Å)	Total number of atom in the system	Simulation temperature (°C)	Simulation time for each MD run (ns)
T-TPC$_6$–0°	4	72	288	0°	142 x 123 x 199	139968	80	100
T-TPC$_{10}$–0°	4	36	144	0°	145 x 100,4 x 157,8	95904	80	100
T-TPC$_6$–60°	4	72	288	60°	142 x 123 x 199	139968	80	100
T-TPC$_{10}$–180°	4	36	144	180°	145 x 100,4 x 157,8	95904	80	100

[a] The simulations are conducted in periodic boundary conditions – the four columns in the systems replicated in space are representative of an infinite bulk system. [b] Each column is composed of 36 (blue) nodes containing, consistent with the experimental model, one **T-TPC$_{10}$** and two **T-TPC$_6$** molecules respectively (see scheme above). [c] Due to the intrinsic symmetry on the *xy* plane, two arrangements were chosen as initial starting configuration for the simulated systems, both consistent with the XRD experiments. [d] The molecules were initially arranged in space consistent with the experimental lattice parameters from XRD – the initial distances between the columnar assemblies and between the molecules in the single columns were slightly increased (≈20% in percentage) to avoid initial local superpositions.

he simulation work was conducted with the AMBER 12 software.[6] The molecular models for the **T-TPC$_6$** and **T-TPC$_{10}$** molecules were created and parametrized according to a well validated procedure adopted in previous studies on self-assembling branched polymers.[7] In particular, the **T-TPC$_6$** and **T-TPC$_{10}$** supermolecules were parametrized according to the "general AMBER force field (GAFF)" (*gaff.dat*).[8]

After preliminary minimization, all systems were initially heated and pre-relaxed for 100 ps of MD simulation in NPT (constant N: number of atoms, P: pressure and T: temperature) periodic boundary conditions to reach the experimental temperature of 80 °C (353 K) and 1 atm of pressure, using a timestep of 1 femtosecond and anisotropic pressure scaling. The four molecular systems (**T-TPC$_{10}$–0°**, **T-TPC$_6$–0°**, **T-TPC$_{10}$–180°** and **T-TPC$_6$–60°**) underwend additional 100 ns of MD simulation under NPT periodic boundary conditions at the experimental temperature of 80 °C and 1 atm of pressure using anisotropic pressure scaling. During this phase, all MD simulations used a time step of 2 femtoseconds, the Langevin thermostat, and a 10 Å cutoff. The particle mesh Ewald[9] (PME) approach was used to treat the long-range electrostatic effects, and the SHAKE algorithm was used on the bonds involving Hydrogen atoms.[10] During the MD simulations all systems reached the equilibrium with good stability. The root mean square deviation (RMSD) and the potential energy (E) data were extracted from the MD trajectories and used to verify the equilibration of the systems during the runs (Fig. S4). The last 50 ns of each MD simulation were considered as representative of the equilibrium, and used for further analysis. Analysis of the lattice parameters (*a*, *b* and *c*) of the equilibrated molecular systems demonstrates very good consistency between the models and the experiments (see Table S3). In particular, in the case of **T-TPC$_{10}$** the deviation of the lattice parameters provided by the MD from the XRD experiments is in the same range of previous similar reports,[4] while it is practically negligible for **T-TPC$_6$** (≈1%, or below).

The coordinates of the centers of mass (CM) of all blue and red groups were extracted from the equilibrated phase MD trajectories with the *ptraj* module of AMBER 12. Given that the average position of the red and blue groups centres projected on the *xy* plane is well consistent with the XRD data (see also Table S3), we were interested in calculating the probability of finding red and blue groups at variance of the distance from the average (most probable) positions – *i.e.*, in a circular area around the average positions. Thus, the *x* and *y* coordinates of red and blue CM groups were merged into single vectors, and the related Gaussian distributions of these groups around their average lattice positions (*i.e.*, the equilibrated distance between blue and red groups in the systems obtained from the MD simulations) were calculated with Matlab 8.0 (Fig. 3e and Fig. 4c in the main paper).[11]

To obtain additional visual insight on the level of structural order/disorder into the equilibrated lattices, the calculated 1D Gaussians (Fig. 3e and Fig. 4c in the main paper) were rotated aroud their axis. The projection on the *xy* plane of the obtained 2D Gaussian distributions were then replicated in space according to the equilibrated lattice parameters from MD obtaining the qualitative plots reported in Fig. S5. These supplementary plots contain the same data of the 1D Gaussians, and provide visual perception of the level of Gaussian superpositions in the lattice, which are directly related to the level of disorder in the structures (they do not provide any information on molecular shape or on orientation (tilting) of the red and blue groups respect to the *xy* plane). Finally, the radial distribution functions (*g(r)*) of the supramolecular cores respect to themselves were calculated with the ptraj module of AMBER 12 to assess the short range order in the assembly along the *z* axis (stacking).

7. Additional data from MD simulations

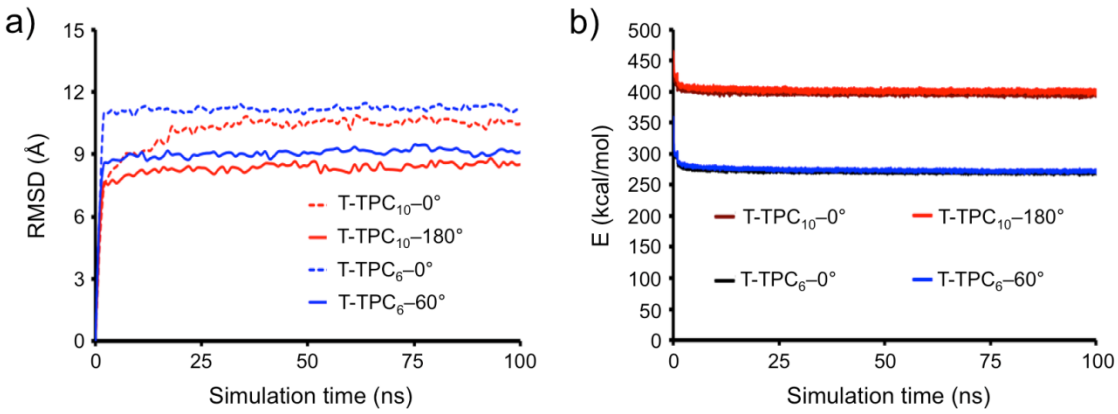

Figure S4. Equilibration of the simulated molecular systems. a) Root mean square displacement data (RMSD) plotted as a function of the simulation time. b) Potential energy of the systems as a function of the simulation time.

Table S3. Lattice parameters for the **T-TPC$_6$** and **T-TPC$_6$** molecular systems obtained from the MD simulations. Data are obtained both for the superimposed (0°) and rotated (60° for **T-TPC$_6$–60°** and 180° for **T-TPC$_{10}$–180°**) equilibrated systems, and compared with the XRD experimental values.

Compound	Experimental Lattice Parameters (Å)	Lattice Parameters from MD (Å) [a] Superimposed (0°)	MD deviation from the XRD experiments [b] Superimposed (0°)	Lattice Parameters from MD (Å) [a] Rotated (60° or 180°)	MD deviation from the XRD experiments [b] Rotated (60° or 180°)
T-TPC$_6$	a = 52.6 Å c = 4.1 Å	a = 52.07 Å c = 4.15 Å	1% 1.2%	a = 52.64 Å c = 4.10 Å	0.7% 0%
T-TPC$_{10}$	a = 80.2 Å b = 58.0 Å c = 3.5 Å	a = 77.41 Å b = 50.31 Å c = 3.38 Å	3.5% 13.8% 3.4%	a = 74.00 Å b = 53.20 Å c = 3.34 Å	7.7% 8.3% 4.6%

[a] The lattice (a, b and c) parameters were obtained from the MD for the equilibrated systems. [b] Percentage deviation of MD equilibrated data from the XRD experiments – for the **T-TPC$_{10}$** case this data is in the same range of previous similar reports,[4] while it is practically negligible in the case of **T-TPC$_6$**.

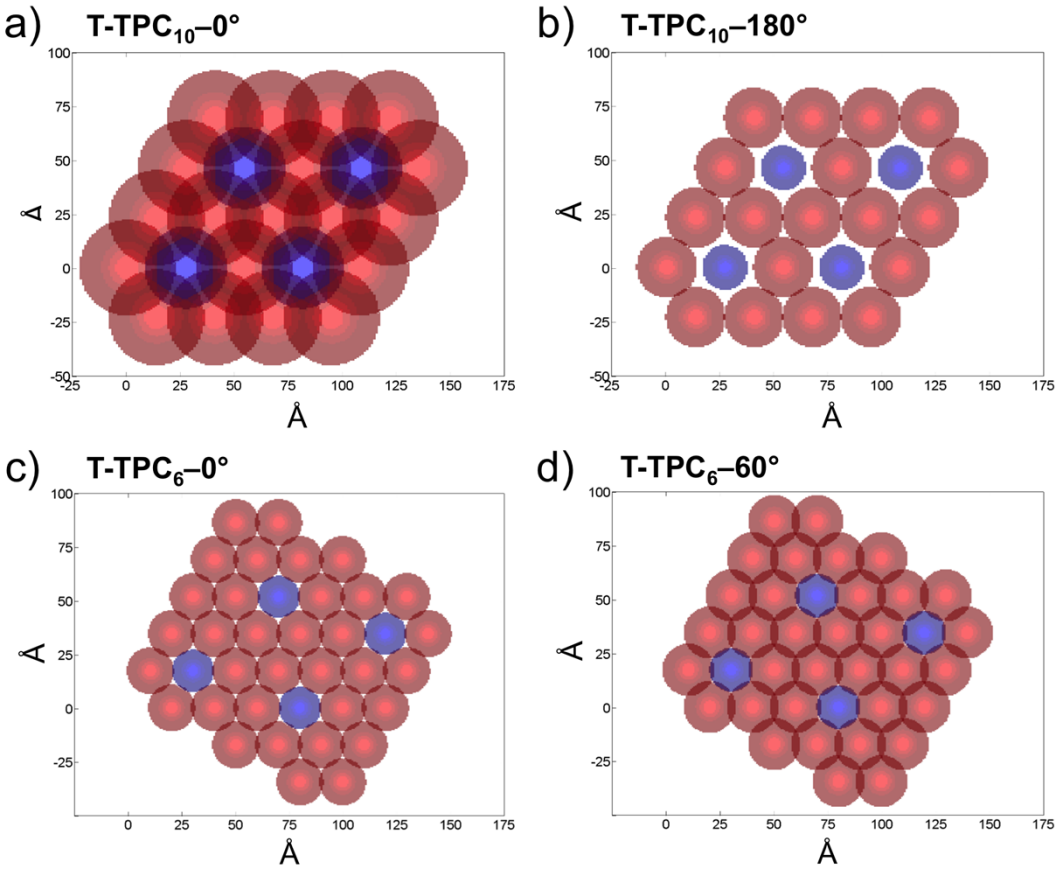

Figure S5. Order on the *xy* plane. The 1D Gaussian probability curves (Fig. 3e and Fig. 4 c in the main paper) related to the displacement on the *xy* plane of the centres of mass (CM) of red and blue groups were rotated around their axis. The projection on the *xy* plane of the obtained 2D Gaussians were replicated in space according to the equilibrated lattice parameters from MD: (a) **T-TPC$_{10}$–0°**, (b) **T-TPC$_{10}$–180°**, (c) **T-TPC$_6$–0°** and (d) **T-TPC$_6$–60°**. The higher the Gaussian superpositions, the higher the level of structural disorder in the equilibrated lattice from MD on the *xy* plane – *i.e.*, the lower the consistency of the assembled configuration (rotated of superimposed) with the XRD experiments.

References

1 H. Strzelecka, C. Jallabert, M. Weber and J. Malthete, *Mol. Cryst. Liq. Cryst.*, 1988, **156**, 347.

2 C. Courme, S. Gillon, N. Gresh, M. Vidal, C. Garbay, J.-C. Florent and E. Bertounesque, *Tet. Lett*. 2008, **49**, 4542.

3 M. Sonoda, A. Inaba, K. Itahashi and Y. Tobe, *Org. Lett.*, 2001, **3**, 2419.

4 X. L. Feng, V. Marcon, W. Pisula, M. R. Hansen, J. Kirkpatrick, F. Grozema, D. Andrienko, K. Kremer and K. Mullen, *Nature Materials*, 2009, **8**, 421.

5 G. Doni, M. D. Nkoua Ngavouka, A. Barducci, P. Parisse, A. De Vita, G. Scoles, L. Casalis and G. M. Pavan, *Nanoscale*, 2013, **5**, 9988.

6 D. A. Case, T. A. Darden, T. E. Cheatham III, C. L. Simmerling, J. Wang, R. E. Duke, R. Luo, R. C. Walker, W. Zhang, K. M. Merz, B. Roberts, S. Hayik, A. Roitberg, G. Seabra, J. Swails, A. W. Goetz, I. Kolossvary, K. F. Wong, F. Paesani, J. Vanicek, R. M. Wolf, J. Liu, X. Wu, S. Brozell, T. Steinbrecher, H. Gohlke, Q. Cai, X. Ye, J. Wang, M.-J. Hsieh, G. Cui, D. R. Roe, D. H. Mathews, M. G. Seetin, R. Salomon-Ferrer, C. Sangui, V. Babin, T. Luchko, S. Gusarov, A. Kovalenko, P. A. Kollman, AMBER 12. In University of California, San Francisco, 2012.

7 (a) D. A. Torres, M. Garzoni, A. V. Subrahmanyam, G. M. Pavan and S. Thayumanavan, J. Am. Chem. Soc., 2014, **136**, 5385; (b) M. Garzoni, N. Cheval, A. Fahmi, A. Danani and G. M. Pavan, J. Am. Chem. Soc., 2012, **134**, 3349; (c) M. Garzoni, K. Okuro, N. Ishii, T. Aida and G. M. Pavan, ACS Nano, 2014, **8**, 904.

8 J. Wang, R. M. Wolf, J. W. Caldwell, P. A. Kollman, D. A. Case, *J. Comput. Chem.*, 2004, **25,** 1157.

9 T. Darden, D. York, L. Pedersen, *J. Chem. Phys.*, 1993, **98**, 10089.

10 V. Krautler, W. F. van Gunsteren, P. H. Hunenberger, *J. Comput. Chem*., 2001, **22**, 501.

11 MATLAB Release 2010a, The MathWorks, Inc., Natick, Massachusetts, United States.